Pattern formation of second harmonic conical waves in a nonlinear medium with extended defect structure

Y. C. Lin, K. W. Su, K. F. Huang, and Y. F. Chen*

Department of Electrophysics, National Chiao Tung University, Hsinchu, Taiwan
*yfchen@cc.nctu.edu.tw

Abstract: We experimentally demonstrate the propagation of the conical second harmonic fields generated from a nonlinear crystal with extended defects to investigate their pattern formation. The generated second harmonic waves are found to be the interference of multiple Bessel-like beams that originate from distinct longitudinal layers inside the crystal. To reconstruct the experimental results, we model the individual Bessel-like beam to be the superposition of an ensemble of identical decentered Gaussian waves with random phases. We present that the randomness of the phases leads the Bessel-like beams to show wave profiles with different extent of localization. Moreover, we use the coherent superposition of the developed wave functions with a phase factor to manifest the interference of multiple Bessel-like beams. The relative phases among the Bessel-like beams are shown to be closely related to the near and far-field patterns. With the experimental observations and the theoretical model, the relative phases are decided to successfully reconstruct the propagation characteristics of the multiple Bessel-like beams.

OCIS codes: (290.4210) Multiple scattering; (030.1670) Coherent optical effects; (190.2620) Harmonic generation and mixing; (140.3480) Lasers, diode-pumped.

References and links

1. G. S. He and S. H. Liu, *Physics of Nonlinear Optics* (World Scientific, 1999).
2. K. D. Moll, D. Homoelle, A. L. Gaeta, and R. W. Boyd, "Conical harmonic generation in isotropic materials," Phys. Rev. Lett. **88**(15), 153901 (2002).
3. S. Trillo, C. Conti, P. Di Trapani, O. Jedrkiewicz, J. Trull, G. Valiulis, and G. Bellanca, "Colored conical emission by means of second-harmonic generation," Opt. Lett. **27**(16), 1451–1453 (2002).
4. A. R. Tunyagi, M. Ulex, and K. Betzler, "Noncollinear optical frequency doubling in strontium barium niobate," Phys. Rev. Lett. **90**(24), 243901 (2003).
5. Y. F. Chen, K. W. Su, T. H. Lu, and K. F. Huang, "Manifestation of weak localization and long-range correlation in disordered wave functions from conical second harmonic generation," Phys. Rev. Lett. **96**(3), 033905 (2006).
6. H. Zeng, J. Wu, H. Xu, K. Wu, and E. Wu, "Colored conical emission by means of second harmonic generation in a quadratically nonlinear medium," Phys. Rev. Lett. **92**(14), 143903 (2004).
7. G. Giusfredi, D. Mazzotti, P. Cancio, and P. De Natale, "Spatial mode control of radiation generated by frequency difference in periodically poled crystals," Phys. Rev. Lett. **87**(11), 113901 (2001).
8. P. Xu, S. H. Ji, S. N. Zhu, X. Q. Yu, J. Sun, H. T. Wang, J. L. He, Y. Y. Zhu, and N. B. Ming, "Conical second harmonic generation in a two-dimensional $\chi^{(2)}$ photonic crystal: a hexagonally poled $LiTaO_3$ crystal," Phys. Rev. Lett. **93**(13), 133904 (2004).
9. S. M. Saltiel, D. N. Neshev, R. Fischer, W. Krolikowski, A. Arie, and Y. S. Kivshar, "Generation of second-harmonic conical waves via nonlinear bragg diffraction," Phys. Rev. Lett. **100**(10), 103902 (2008).
10. W. Wang, Y. Sheng, Y. Kong, A. Arie, and W. Krolikowski, "Multiple Čerenkov second-harmonic waves in a two-dimensional nonlinear photonic structure," Opt. Lett. **35**(22), 3790–3792 (2010).
11. J. Chen and X. Chen, "Phase matching in three-dimensional nonlinear photonic crystals," Phys. Rev. A **80**(1), 013801 (2009).
12. L. Mateos, P. Molina, J. Galisteo, C. López, L. E. Bausá, and M. O. Ramírez, "Simultaneous generation of second to fifth harmonic conical beams in a two dimensional nonlinear photonic crystal," Opt. Express **20**(28), 29940–29948 (2012).

#223077 - $15.00 USD Received 15 Sep 2014; revised 24 Oct 2014; accepted 26 Oct 2014; published 3 Nov 2014

13. Y. C. Lin, P. H. Tuan, Y. T. Yu, H. C. Liang, K. W. Su, K. F. Huang, and Y. F. Chen, "Observation of disordered wave functions with conical second-harmonic generation and verification of transition from extended to prelocalized states in weak localization," Phys. Rev. B **87**(4), 045117 (2013).
14. F. Gori, G. Guattari, and C. Padovani, "Bessel-Gauss beams," Opt. Commun. **64**(6), 491–495 (1987).
15. V. Bagini, F. Frezza, M. Santarsiero, G. Schettini, and G. S. Spagnolo, "Generalized bessel-gauss beams," J. Mod. Opt. **43**, 1155 (1996).
16. M. Janssen, *Fluctuations and Localization in Mesoscopic Electron Systems* (World Scientific, 2001).
17. K. Efetov, *Supersymmetry in Disorder and Chaos* (Cambridge University, 1997).
18. P. Sheng, *Introduction to Wave Scattering, Localization and Mesoscopic Phenomena* (Springer, 2006).
19. A. Ishimaru, *Wave Propagation and Scattering in Random Media* (IEEE, 1997).
20. M. L. Sosnowska, E. Olszyńska, A. Pajączkowska, and A. Kłos, "Extended defects in $GdCa_4O(BO_3)_3$ crystals," J. Cryst. Growth **262**(1-4), 388–394 (2004).
21. H. Wei and H. Xu, "Hot spots in different metal nanostructures for plasmon-enhanced Raman spectroscopy," Nanoscale **5**(22), 10794–10805 (2013).
22. A. Kudrolli, V. Kidambi, and S. Sridhar, "Experimental studies of chaos and localization in quantum wave functions," Phys. Rev. Lett. **75**(5), 822–825 (1995).
23. M. Moshinsky, "Diffraction in time," Phys. Rev. **88**(3), 625–631 (1952).
24. Č. Brukner and A. Zeilinger, "Diffraction of matter waves in space and in time," Phys. Rev. A **56**(5), 3804–3824 (1997).
25. Th. Hils, J. Felber, R. Gähler, W. Gläser, R. Golub, K. Habicht, and P. Wille, "Matter-wave optics in the time domain: Results of a cold-neutron experiment," Phys. Rev. A **58**(6), 4784–4790 (1998).
26. A. Goussev, "Huygens-Fresnel-Kirchhoff construction for quantum propagators with application to diffraction in space and time," Phys. Rev. A. **85** 013626 (2012).
27. P. O'Connor, J. Gehlen, and E. J. Heller, "Properties of random superpositions of plane waves," Phys. Rev. Lett. **58**(13), 1296–1299 (1987).
28. A. E. Siegman, *Lasers* (University Science Books, 1986).
29. G. B. Arfken and H. J. Weber, *Mathematical Methods for Physicists* (Academic, 2001).
30. J. Durnin, J. Miceli, Jr., and J. H. Eberly, "Diffraction-free beams," Phys. Rev. Lett. **58**(15), 1499–1501 (1987).
31. L. Pitaevskii and S. Stringari, "Interference of bose-einstein condensates in momentum space," Phys. Rev. Lett. **83**(21), 4237–4240 (1999).

1. Introduction

Second harmonic generation (SHG) is one of the parametric processes that have been intensively studied in nonlinear optics [1]. It has been realized by a variety of methods involving with the phase-matching relations between interacting waves, and the types of nonlinear media. The most usual scheme of SHG is regarded to be collinear which signifies that all contributing light beams are pointing approximately into the same direction [1]. The advantage of such collinear geometries is the large interaction lengths which significantly enhance the efficiency of the frequency conversion. However, SHG is not restricted to the collinear interactions; non-collinear schemes can be realized as well. Though the non-collinear geometries are not suitable for efficient frequency doubling, scientists have taken great interests in their physics and applications on material characterization [2–13].

Several kinds of non-collinear parametric interactions have been recently demonstrated, such as a conical third-harmonic emission generated in an isotropic material [2], a hollow beam generated by the frequency difference in a periodically poled $LiNbO_3$ crystal [7], and a conical SH beam discovered in a two-dimensional (2D) hexagonally poled $LiTaO_3$ crystal [8]. Studies have shown that the conical SH beams can be generated from nonlinear media with different order photonic structures through the quasi-phase-matching technique [7–12]. However, it is not necessary to work with order photonic structures; the conical SH patterns can even be produced in a disordered nonlinear crystal [4]. More recently, the near-field conical patterns in a nonlinear crystal with extended defects have been measured to manifest the weak localization and long-range correlation in disordered wave functions [5]. The conical patterns have recorded the spatial distribution of the scattering signal and disclosed the structure information and symmetry of the random medium. This indicates that the pattern formation of the conical beams deserves profound investigation to understand the topological characteristics of the medium. Nevertheless, so far there have been few studies focused on the pattern formation of the conical beams due to the lack of accessibility.

In this work, we present the first experimental results of the propagation of the conical SH fields generated from a nonlinear crystal with extended defects to systematically explore their pattern formation. The experimental setup is the same as [5] where a $GdCa_4O(BO_3)_3$

#223077 - $15.00 USD Received 15 Sep 2014; revised 24 Oct 2014; accepted 26 Oct 2014; published 3 Nov 2014

(GdCOB) sample is used as the nonlinear crystal to perform the intra-cavity SHG in a Q-switched Nd:YAG laser. We generate various conical patterns by thoroughly scanning different transverse positions in the GdCOB crystal. We discover that the generated SH waves are composed of multiple Bessel-like beams that originate from distinct longitudinal layers inside the crystal. Each Bessel-like beam is found to preserve its profile for a certain distance, which enables the generated SH waves to exhibit interference in the near and far-field regimes. Furthermore, we theoretically prove that the individual Bessel-like field can be expressed as an ensemble of identical decentered Gaussian waves [14,15] with random phases. We model the interference of multiple Bessel-like beams to be a coherent superposition of the developed wave functions with a phase factor. With the experimental results and the developed model, we determine the relative phases between the wave functions to successfully reconstruct the near-field patterns and their propagation behavior. The present results manifest the significance of the relative phases in the pattern formation due to the longitudinal separations and might provide some useful insights into the localization phenomena of scattered waves passing through random media [16–19].

2. Experimental observations

Figure 1 shows the experimental setup of a diode-pumped actively Q-switched Nd:YAG laser with intracavity SHG in a GdCOB crystal. The same experimental scheme has been presented in [5,13]. The active medium is a 0.8-at. % Nd^{3+}:YAG crystal with a length of 10 mm. The GdCOB crystal was cut for type I frequency doubling in the XY planes ($\theta = 90°$, $\varphi = 46°$) with a length of 2 mm and a cross section of 3 mm × 3 mm. All crystals were coated for antireflection (R<2%) at 1064 nm on their both sides. The radius of curvature of the concave-front mirror is 50 cm with coating of antireflection (R<0.2%) at 808 nm, high-reflection (R>99.8%) at 1064 nm, and 532 nm on the entrance side and high-transmission (T>90%) at 808 nm on the other side. The output coupler is a plane mirror with coating of high-reflection (R>99.8%) at 1064 nm and high-transmission at 532 nm (T>85%). The pump source is a 10 W 808 nm fiber-coupled laser diode with a core diameter of 800 μm. A focusing lens with a focal length of 2.5 cm and 90% coupling efficiency was employed to reimage the pump beam into the laser gain medium. The acoustic-optic Q switch (NEOS Model 33027-15-2-1) with a length of 30 mm has coating of antireflection at 1064 nm on both sides and was driven at a 27.12-MHz center frequency with 15.0 W of rf power. A high-resolution microscope was used to reimage the near-field patterns on the screen. The SH field is formed by both the collinear ($\vec{k}_1 + \vec{k}_1 = \vec{k}_2$) and non-collinear interactions. Therefore, there are two components including an on-axis beam and a conical beam in the resulting pattern. To clearly observe the conical beam without the influence of the on-axis one, we stuck a circular object on the center of the microscope to obstruct the propagation of the on-axis beam.

Since the nonlinear GdCOB crystal possesses extended defect domains [20], the fundamental wave is randomly scattered by numerous defects. When an axial fundamental field $\vec{k}_1$ and a scattered field $\vec{k}_1'$ satisfy the phase-matching condition $\vec{k}_1 + \vec{k}_1' = \vec{k}_2$, a decentered SH field with wave vector $\vec{k}_2$ can be generated to form a conical SHG process. Figure 2(a) indicates the phase-matching diagram for the conical SHG process, where the cone angle β with respect to the *z* axis is decided by the effective refractive indices and $\vec{\kappa}$ is the transverse component of the wave vector $\vec{k}_2$ with $\kappa = k_2 \sin\beta$. Localization of the fundamental wave scattered by the defects in the crystal leads to the so-called hot-spots [21], the tiny areas with greatly enhanced electromagnetic field and cause the SH field to reveal the features of disordered wave functions [22].

#223077 - $15.00 USD Received 15 Sep 2014; revised 24 Oct 2014; accepted 26 Oct 2014; published 3 Nov 2014

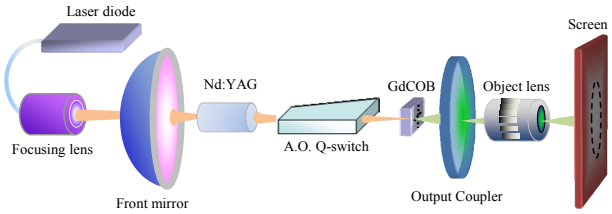

Fig. 1. Experimental setup for the generation of conical SH waves in a diode-pumped Q-switched Nd:YAG laser.

Since the distribution of the random defects significantly depends on the transverse position of the nonlinear crystal, a variety of SH waves can be observed by scanning different transverse positions [5]. The simplest wave pattern in the SH field is like a single multi-ringed wave whose spatial structure is similar to a zero-order Bessel beam with a Gaussian envelope, as shown in Fig. 2(b). The propagation evolution and far-field pattern for the Bessel-like beam are shown in Figs. 2(c)-2(e). Previous works have shown that the free-space propagation of lasing modes can be employed to analogously study the quantum transient dynamics for the diffraction-in-time effect in matter waves [23–26]. The propagation of the wave field presented in Figs. 2(c)-2(e) could provide some insight into the investigation on the quantum transient phenomenon. Moreover, the cone angle β of the far-field pattern shown in Fig. 2(f) is directly related to the phase-matching angle which is determined by the effective refractive indices of the nonlinear crystal. It is worth mentioning that there should be an on-axis beam resulting from the collinear interaction in Fig. 2(f). However, a circular object was employed to block the on-axis beam, preventing its influence on the observation of the conical one. Thus, one can see a circular shadow in the center. Light around the circular shadow is also observed since the on-axis beam is not completely obscured by the object.

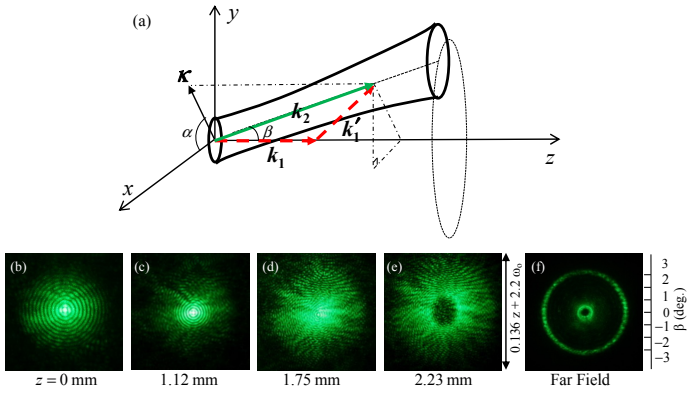

Fig. 2. (a) Schematic diagram for the phase-matching condition of the conical SHG process, where $\vec{k}_1$ and $\vec{k}_1'$ are the wave vectors for the axial and scattered off-axis fundamental fields, and $\vec{k}_2$ is the wave vector for the phase-matched decentered SH field. (b)-(f) Experimental results for the propagation of the generated SH wave.

In general, the observed SH waves can be decomposed into the coherent superposition of several Bessel-like beams. Figure 3 displays the SH wave patterns that consist of two, four, and six Bessel-like beams which stem from the hot-spots at distinct longitudinal and transverse positions inside the nonlinear crystal, as illustrated schematically in Fig. 3(a). The longitudinal distances for the hot-spots can be estimated by employing the high-resolution microscope to observe the separations between the optimal focal planes of the Bessel-like beams. Distances among the hot-spots are measured to be around 10-20 μm. The coherence phenomenon can exhibit between the Bessel-like beams since the longitudinal separations are

#223077 - $15.00 USD Received 15 Sep 2014; revised 24 Oct 2014; accepted 26 Oct 2014; published 3 Nov 2014

rather short to be compared to the Rayleigh range of the individual one, as seen in Fig. 3. The Rayleigh range for the Bessel-like beam is calculated to be about 4 cm in length with the formula of Rayleigh range $z_R = k_2\,\omega_o^2 / 2$, where $k_2 = 2\pi/\lambda$ is the wave number with the optical wavelength $\lambda = 0.532\,\mu\text{m}$ and $\omega_o \sim 80\,\mu\text{m}$ is the beam waist of the generated SH wave. The multiple Bessel-like beams nearly preserve their profiles through a certain longitudinal distance to interfere in the near-field regime, which enables the generated SH waves to exhibit complex interference patterns. The interference is simultaneously observed in the far-field patterns which display single-ringed profiles with fringes corresponding to the varying near-field distributions, as shown in Figs. 3(f), 3(k), and 3(p).

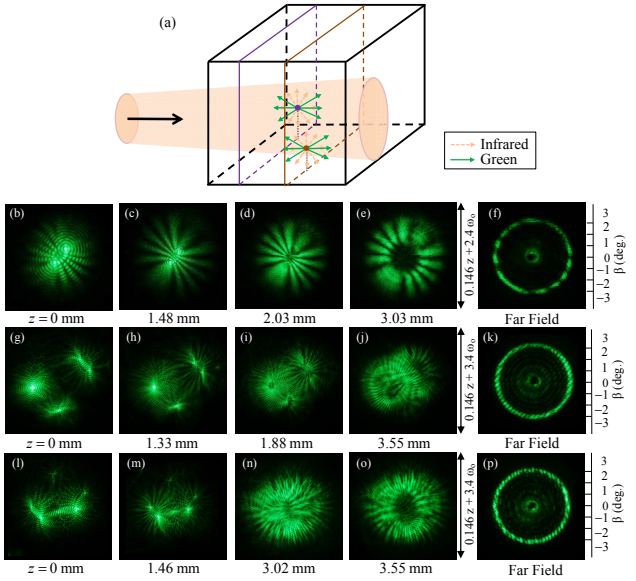

Fig. 3. (a) Schematic diagram for the fundamental input beam passing through scatters to form two hot-spots located on different layers, where the dashed arrows and the solid arrows signify the wave vectors of the fundamental and the SH fields. (b)-(p) Propagation of various experimental SH waves.

Figure 4 demonstrates another kind of SH wave pattern formed by the interference of dozens of Bessel-like beams that originate randomly from different layers inside the crystal. This SH wave pattern has been called the extended state which has its intensity distribution widely spreading over the space [5,13]. It is clear seen that the extended state displays the propagation behavior of the random pattern associated with the quasi-linear ridge structure [27]. In the following section we construct an analytical model to make a further understanding for the morphologies of these SH fields and the coherence phenomena between the composite Bessel-like beams.

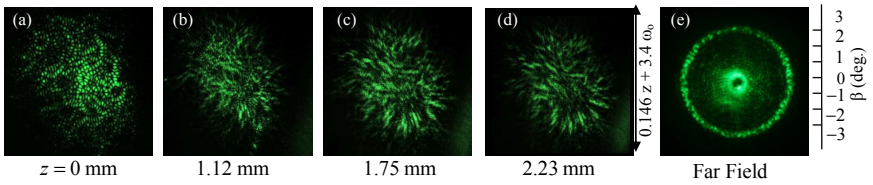

Fig. 4. Propagation of the experimental extended state.

#223077 - $15.00 USD Received 15 Sep 2014; revised 24 Oct 2014; accepted 26 Oct 2014; published 3 Nov 2014

3. Analytical model for conical beams

To develop an analytical model for the generated SH fields, we use decentered Gaussian beams as basis to reconstruct the wave functions that form the SH patterns. The near-field wave function u_o of the decentered SH Gaussian beam in terms of the cylindrical coordinates (r,ϕ) can be expressed as [28]

$$u_o(r,\phi;\alpha)=\exp\left[-\left(\frac{r}{\omega_o}\right)^2\right]\exp\left[i\kappa r\cos(\alpha-\phi)\right], \tag{1}$$

where ω_o is the beam waist of u_o at plane $z=0$ and α is the azimuthal angle between $\bar{\kappa}$ and the positive x axis. In terms of the first kind Bessel function of zero order [29], the integration of the wave function u_o over the entire azimuthal angle α is the *so-called* Bessel-Gauss (BG) beam:

$$U_{BG}(r,\phi)=\int_0^{2\pi}u_o(r,\phi;\alpha)\,d\alpha=2\pi\exp\left(-\frac{r^2}{\omega_0^2}\right)J_0(\kappa r). \tag{2}$$

The BG beam is first proposed by Gori and Guattari to overcome the difficulties of the realization of diffraction-free beams [30]. The wave function U_{BG} can be treated as the coherent superposition of an ensemble of the Gaussian beams u_o with identical phase. Although the BG beam can display profile similar to the experimental result in Fig. 2(b), the asymmetric SH pattern due to the random scattering process cannot be manifested. In this case, we add a random phase factor to the wave function u_o to closely model the asymmetric feature in the pattern. The assumption of the random phase can be traced back to the previous work by O'Connor, Gehlen, and Heller [27], in which they investigate the random eigenfunctions of a classically chaotic system. The behaviors of the random eigenfunctions are found to be well interpreted as the superposition of monochromatic plane waves with random directions, amplitudes, and phases. Riemann sum is exploited to obtain the total field since definite integral cannot be solved with the random phases. The total field is thus given by

$$U_o(r,\phi;\Delta)=\sum_{q=0}^{M-1}\exp(i\theta_q)u_o(r,\phi;\alpha_q)\ \frac{2\pi}{M}, \tag{3}$$

where $\alpha_q=2\pi q/M$, $q=0\ldots M-1$, $|\theta_q|\le\Delta/2$, Δ is an arbitrary constant to define the range of the random phases θ_q with $\Delta\le 2\pi$, and M is the total number of the composite Gaussian beams. The random phases θ_q corresponding to each Gaussian beams are generated in the range from $-\Delta/2$ to $\Delta/2$ by the method of simple random sampling. The deviation of the random phases is simultaneously decided by the range Δ and the number of composite Gaussian waves, M. As $M\to\infty$ and $\Delta=0$, the wave function U_o reduces to U_{BG}.

Figures 5(a)-5(e) display various simulated results of U_o by changing the values of Δ for the random phases. Since numerical analyses exhibit that a superposition of 300 Gaussian waves is already sufficient to reconstruct the wave features of the wave function U_o, the presented results are all simulated by the number of Gaussian waves, each with the beam waist of $\omega_o=80\,\mu\text{m}$ according to the experimental configuration. Due to the relation $\kappa=k_2\sin\beta$, we estimate the magnitude of $\kappa\approx 0.618$ rad. with $k_2=11.81\,\text{um}^{-1}$ and

#223077 - $15.00 USD Received 15 Sep 2014; revised 24 Oct 2014; accepted 26 Oct 2014; published 3 Nov 2014

$\beta \approx 0.052$ rad. (3 deg.), which are obtained from the phase-matching condition and the experimental observations in Figs. 2-4, respectively. It can be seen that the simulated patterns transform from a symmetric BG beam to a chaotic pattern of a network of quasi-linear ridge structure [27] as Δ becomes larger. The simulated near-field distribution in Fig. 5(b) successfully manifests the experimental result in Fig. 2(b). The investigation suggests that the random phase plays a dominant role in reconstructing the morphologies of the wave functions.

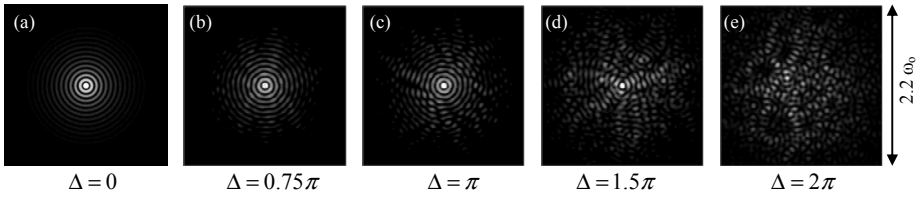

Fig. 5. (a)-(e) Theoretical simulations of $U_o(r,\phi;\Delta)$ with Δ varying from 0 to 2π.

With the near-field distribution U_o, the z-dependent wave function $U(r,\phi,z;\Delta)$ can be expressed in terms of the Fresnel diffraction integral [28]:

$$U(r,\phi,z;\Delta)=\frac{k_2\exp(i\,k_2\,z)}{i\,2\pi\,z}\int_0^{\infty}\int_0^{2\pi}U_o(r',\phi';\Delta)\exp\left(i\frac{k_2\,|\vec{r}-\vec{r}'|^2}{2\,z}\right)r'\,d\phi'\,dr'. \quad (4)$$

Substituting Eq. (3) into Eq. (4), we obtain

$$U(r,\phi,z;\Delta)=\sum_{q=0}^{M-1}\exp(i\,\theta_q)\,u(r,\phi,z;\alpha_q)\frac{2\pi}{M}, \quad (5)$$

with

$$\begin{aligned}u(r,\phi,z;\alpha_q)=&\frac{\omega_o}{\omega(z)}\exp\left\{i\left[k_2\,z-\frac{\kappa^2 z}{2k_2}-\Phi(z)\right]\right\}\\&\times\exp\left\{-F(z)\left[r^2+\left(\frac{\kappa z}{k_2}\right)^2-2\frac{\kappa z\,r}{k_2}\cos(\alpha_q-\phi)\right]\right\},\\&\times\exp\left[i\,\kappa r\cos(\alpha_q-\phi)\right]\end{aligned} \quad (6)$$

where $\omega(z)=\omega_o\sqrt{1+(z/z_R\cos\beta)^2}$ is the beam radius at plane z, $\Phi(z)=\tan^{-1}(z/z_R\cos\beta)$ is the Gouy phase, $F(z)=[1/\omega(z)^2]-[i\,k_2/2R(z)]$, and $R(z)=[z/\cos\beta]+[z_R{}^2\cos\beta/z]$ is the radius of curvature. The wave function u is the z-dependent expression of the decentered SH Gaussian beam propagating at an angle β with respect to the z axis. Figure 6 demonstrates the simulations of the propagation for the wave function in Fig. 5(b), where the theoretical results display good agreement with the experimental observations in Figs. 2(b)-2(f). The transverse patterns are shown to diverge radially along the longitudinal direction and finally form the ring structure in the far-field regime.

#223077 - $15.00 USD Received 15 Sep 2014; revised 24 Oct 2014; accepted 26 Oct 2014; published 3 Nov 2014

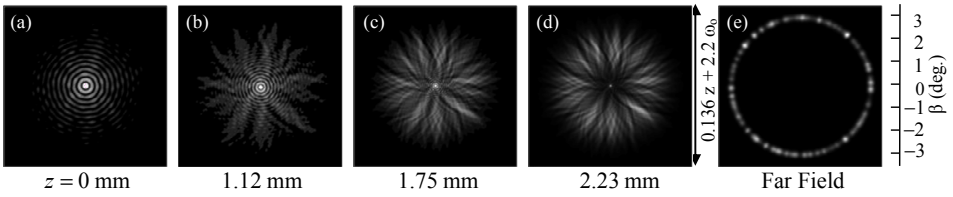

Fig. 6. (a)-(e) Reconstructed patterns $U(r,\phi,z;\Delta)$ for the propagation of the experimental results in Figs. 2(b)-2(f).

To reconstruct the SH field that consist of multiple Bessel-like beams, we model the near-field distribution of the SH wave to be the coherent superposition of U_o:

$$V_o(r,\phi)=\sum_{n=0}^{N-1}\exp(i\delta_n)\,U_{on}\left(\left|\vec{r}-\vec{r}_n\right|,\phi;\Delta_n\right), \tag{7}$$

where δ_n is a phase factor for the *n*th Bessel-like beam U_{on}, $\delta_n = k_2 l_n$, l_n is the longitudinal displacement from the reference plane at $z=0$ to where U_{on} is originated. The reference plane is defined at the beam waist of U_{oo}, and therefore δ_o is equal to zero. $\vec{r}_n = (x_n, y_n)$ is the transverse coordinates relative to the beam axis for the position U_{on} is originated, and *N* is the total number of the composite Bessel-like beams. With Eq. (4), the propagation of the distribution V_o can be expressed as

$$V(r,\phi,z)=\sum_{n=0}^{N-1}\exp(i\delta_n)\,U_n\left(\left|\vec{r}-\vec{r}_n\right|,\phi,z;\Delta_n\right). \tag{8}$$

The influence of δ_n on the interference phenomena between two Bessel-like beams U_n is illustrated in Fig. 7, where Figs. 7(a)-7(e) are the near-field distributions for different δ_1, and Figs. 7(f)-7(j) are their far-field counterparts. It is clearly seen that the varying δ_1 are related to distinct near and far-field patterns. The investigation indicates that the best fits for the relative phases δ_1 can be determined by the experimental observations of the wave patterns.

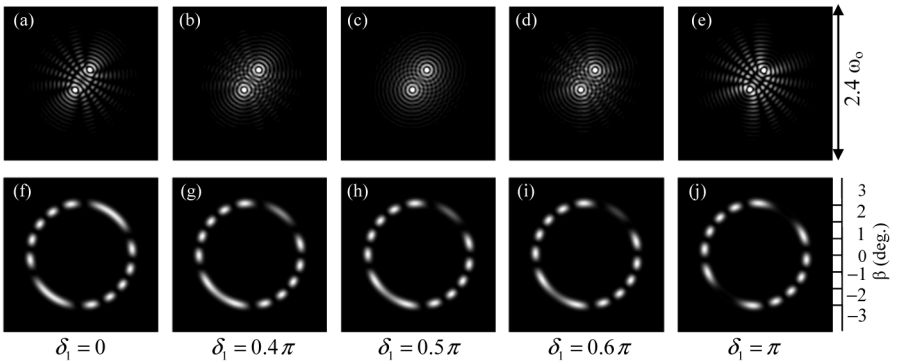

Fig. 7. (a)-(e) Theoretical simulations of $V_o(r,\phi)$ for two Bessel-like beams that originate from different layers. (f)-(j) Corresponding far-field simulations of the distributions $V(r,\phi,z)$.

#223077 - $15.00 USD Received 15 Sep 2014; revised 24 Oct 2014; accepted 26 Oct 2014; published 3 Nov 2014

Computed with the wave function V in Eq. (8), the SH waves in Fig. 3 are successfully reconstructed, as depicted in Fig. 8. The composite wave functions U_n are all simulated by the superposition of 300 Gaussian waves, each with a random phase generated in the range of $-0.25\pi \sim 0.25\pi$, i.e. $\Delta_n = 0.5\pi$. From careful observations of the experimental patterns, the best fits for δ_n are $\delta_1 = 0.26\pi$ for the two Bessel-like beams in Fig. 8(a), $\delta_1 = 0.4\pi$, $\delta_2 = 0$, and $\delta_3 = 0.7\pi$ for the ones from the left to the right in Fig. 8(f), and $\delta_1 = \delta_2 = \delta_3 = \delta_4 = \delta_5 = 0$ in Fig. 8(k). The similarity between the experimental results in Fig. 3 and the simulation in Fig. 8 can be quantified by the overlap integral having the form

$$S = \iint \sqrt{I_{\exp}(x,y)}\sqrt{I_{sim}(x,y)}\, dx\, dy, \tag{9}$$

where $I_{\exp}$ and I_{sim} are the normalized intensity distributions for the experimental and simulated near-field patterns, respectively. For ideal case of $I_{\exp} = I_{sim}$, S can be directly evaluated to be 1. The larger the value of S is, the better the similarity is. The values of S are calculated to be 0.87, 0.84, and 0.82 for near-field patterns in Figs. 3(b) and 8(a), Figs. 3(g) and 8(f), and Figs. 3(l) and 8(k), respectively. The good agreement suggest the possibility of measuring the far-field (momentum) distribution to diagnose the topological characterization of the 3D random medium in which Bessel-like beams are formed naturally at distinct layers. The exploration might also provide condensed matter physicists some useful insight into exploring the coherence properties [31] between condensates in the 3D scheme by the direct measurement of the momentum distributions.

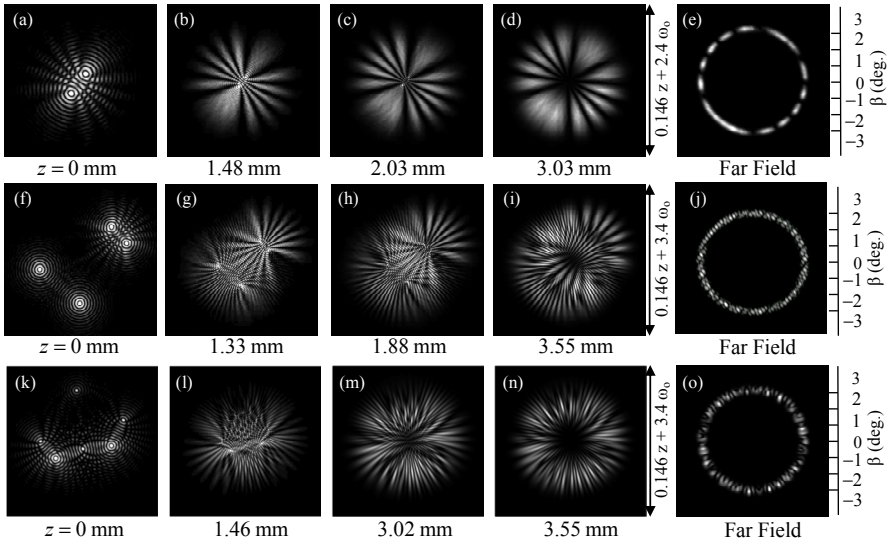

Fig. 8. Theoretical simulations for the experimental results in Fig. 3.

Furthermore, we reconstruct the extended state in Fig. 4 by the superposition of dozens of Bessel-like beams that stem from distinct positions inside the nonlinear crystal, as illustrated schematically in Fig. 9(a). It is clearly seen that the numerical results in Figs. 9(b)-9(f) successfully manifest the propagation characteristics of the extended state. For simplicity, all the wave functions U_n that contribute to V in Eq. (8) are simulated with the identical parameters $M = 300$ and $\Delta_n = 0.5\pi$. Since the spatial interference for the diffraction of light has good analogy to the quantum interference for the diffraction-in-time effect of matter

#223077 - $15.00 USD Received 15 Sep 2014; revised 24 Oct 2014; accepted 26 Oct 2014; published 3 Nov 2014

waves [23–26], the presented results could also be employed to analogously study the transient dynamics of matter waves diffracted with time-varying obstacles

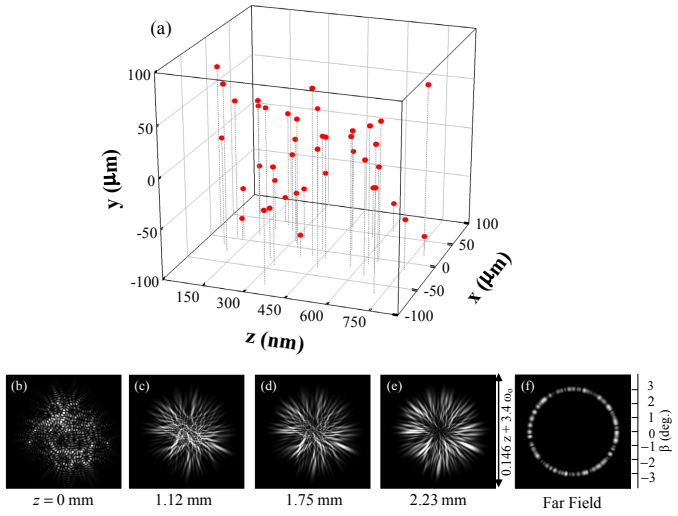

Fig. 9. (a) Schematic diagram for the hot-spots that randomly spread in the 3D nonlinear medium. (b)-(f) Corresponding theoretical simulations of the extended state in Fig. 4.

4. Conclusions

In summary, we have experimentally and theoretically manifested the propagation behavior of conical SH beams to systematically investigate their pattern formation in the nonlinear crystal with extended defects. We have constructed an analytical model to make a comprehensive study of the morphologies and coherence properties for the multiple Bessel-like beams. With the developed model, we have shown that the individual wave function $U(r,\phi,z;\Delta)$ can be expressed as a superposition of identical decentered Gaussian beams $u(r,\phi,z)$ with random phases θ in the range from $-\Delta/2$ to $\Delta/2$. Furthermore, we have employed the coherent superposition of the individual wave functions $U(r,\phi,z;\Delta)$ with the phase factor δ to model the multiple Bessel-like beams. The phase factor δ was shown to be closely connected to the near and far-field patterns. With the theoretical model and the experimental observations, the phases δ were precisely determined to reconstruct the near-field distributions $V_o(r,\phi)$. The propagation of the wave function $V_o(r,\phi)$ has been obtained to show good agreement with the various SH waves. The good agreement indicates that the developed wave functions can be exploited to analyze the topological characterization of a 3D random medium and to analogously study the localization phenomena of scattered waves passing through the random media.

Acknowledgments

The author thanks the National Science Council for their financial support of this research under Contract No. NSC100-2628-M-009-001-MY3.